Electronic Supplementary Material (ESI) for Physical Chemistry Chemical Physics.


# Direct electrical transport measurement on single thermoelectric nanowire embedded in alumina template

**Meriam Ben Khedim,**[1, 2,3] **Laurent Cagnon,**[1, 2] **Christophe Garagnon,**[3] **Valerie Serradeil,**[3] **and Daniel Bourgault** [1,2]

[1]CNRS, Inst. NEEL, F-38042 Grenoble, France

[2]Univ.Grenoble Alpes, Inst. NEEL, F-38042 Grenoble, France

[3]Technology R&D, STMicroelectronics, 13106 Rousset, France

## ELECTRONIC SUPPLEMENTARY INFORMATION

Electrodeposition is considered as the best alternative to vacuum based methods due to its simplicity, rapidity, and low cost. In addition, compounds composition and quality can be controlled by adjusting the initial electrolytes concentration [1] and by varying parameters of pulsed potential deposition. Pure aluminum disks were anodized, at 40 V in oxalic acid electrolyte at 15°C, in order to form nanoporous anodic alumina membranes serving as template material allowing high aspect ratio structures production [2, 3]. Two-step anodization process was used to ensure highly ordered pore arrays.

### Preleminary electrochemical investigation and growth rate characterization

Open-circuit potential was used as the rest potential for the pulsed potential deposition. A metallization was performed on the back side of the membrane by sputtering a 10 nm Ti buffer layer before a 200 nm thick Au layer for the working electrode of the electrodeposition process carried out in a conventional three electrodes cell. A saturated calomel electrode was used as a reference, and a platinum mesh as a counter electrode. All the reported potentials are quoted versus SCE. Preliminary experiments were performed using cyclic voltammetry coupled to an electrochemical quartz crystal microbalance (EQCM, QCM25, Stanford Research Systems) in order to determine the deposition potential range in the above mentioned electrolytes. Figure 1

shows cyclovoltamograms associated with the frequency change of the Au-coated quartz crystal working electrode.

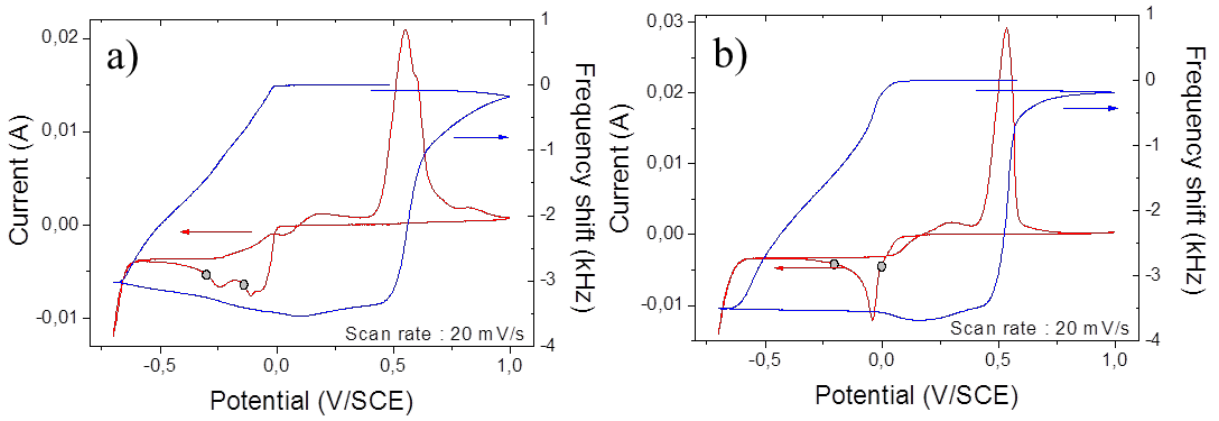


**Figure 1** : Cyclovoltamograms and corresponding EQCM curves obtained in $Bi_{2-x}Sb_xTe_3$ solution (a), and $Bi_2Te_{3-x}Se_x$ solution (b).

As can be seen on the frequency curves, bulk deposition starts around 0 V in both solutions. The chosen deposition potentials are indicated with a grey dot. We therefore have investigated the deposition rates obtained at these potentials. Our approach consisted in comparing SEM cross section observations of membranes after 2 hours of deposition and the mass obtained within the first 10s of deposition which correspond to $t_{on}$ in our pulsing sequence. Figure 2 displays current transients, coupled with the mass variation of our Au-coated quartz crystal working electrode, obtained in the p- and n-type solutions in potentiostatic mode. Figure 3 displays cross-section images, obtained with backscattered electrons, of membranes after 2 hours of deposition at the considered potentials.

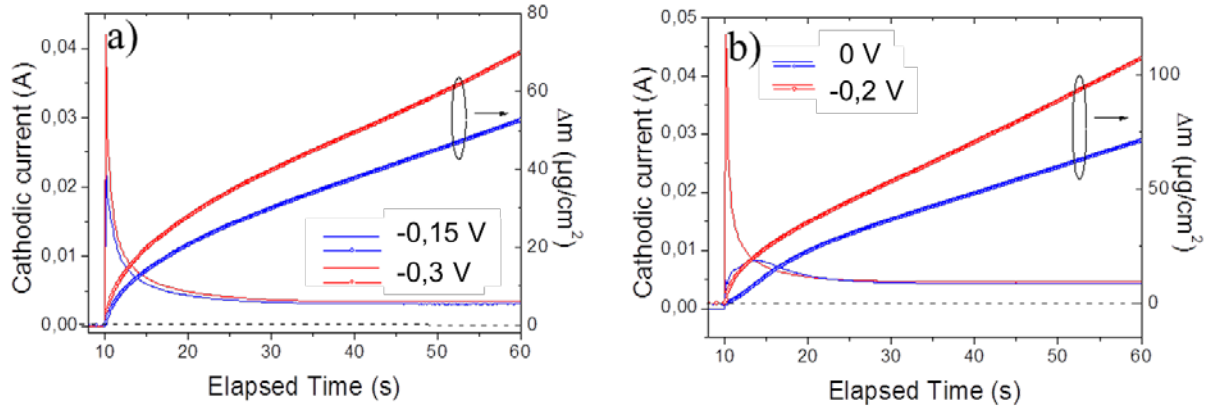


**Figure 2** : I-t and Δm-t curves obtained in $Bi_{2-x}Sb_xTe_3$ solution (a), and $Bi_2Te_{3-x}Se_x$ solution (b) for the different deposition potentials used.

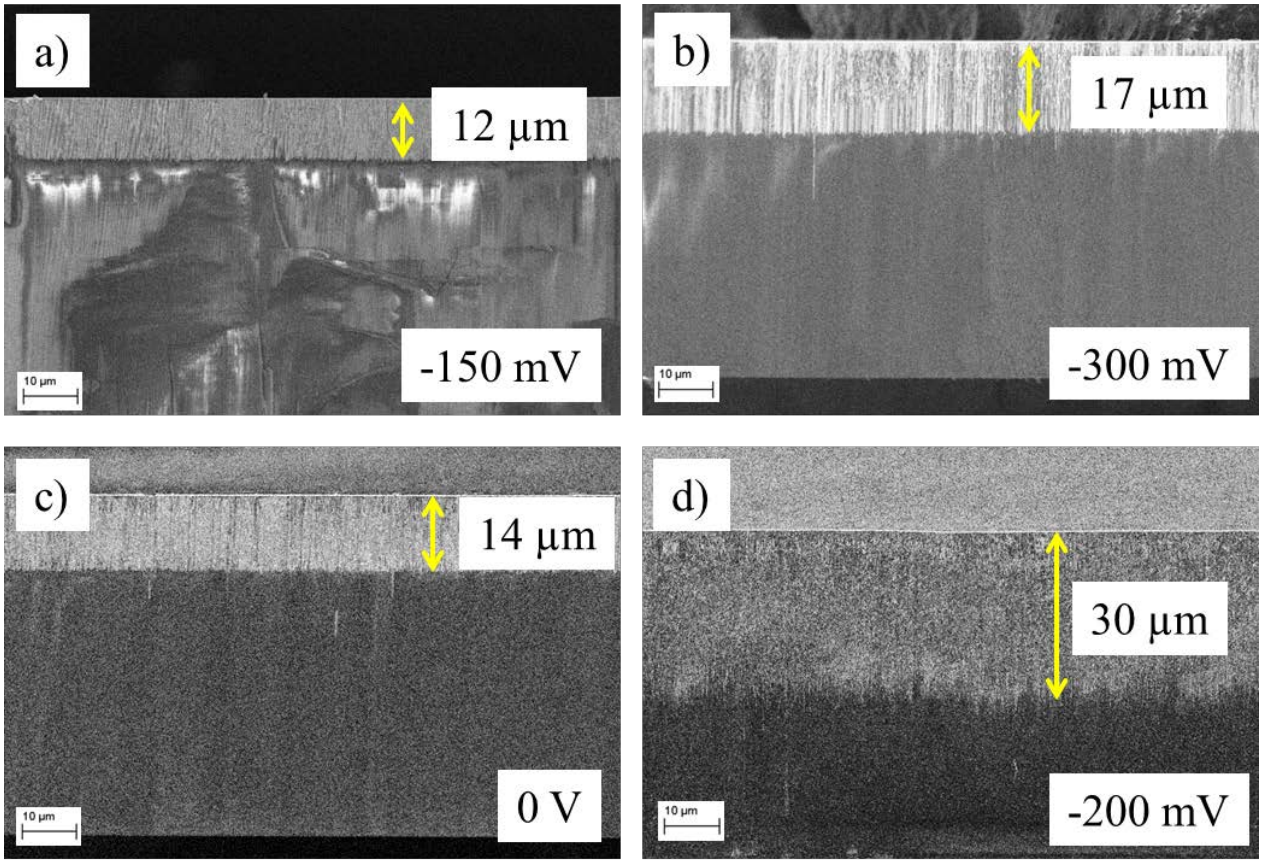


**Figure 3** : SEM cross-section (EBSD mode) images showing the membrane filling after 2 hours deposition in $Bi_{2-x}Sb_xTe_3$ solution (a, b), and $Bi_2Te_{3-x}Se_x$ solution (c, d).

As can be seen on figure 2, in both cases, the steady current values reached are very close. On the other hand, the mass variation is always larger for the most negative deposition potential. Table 1 gathers the nanowires lengths measured on the SEM images of figure 3 and the Δm values reached after 10 s of deposition from figure 2.

| | $Bi_{2-x}Sb_xTe_3$ | | $Bi_2Te_{3-x}Se_x$ | |
|---|---|---|---|---|
| $U_d$ (V/SCE) | -0.15 | -0.3 | 0 | -0.2 |
| $l_{SEM}$ (µm) | 12 | 17 | 14 | 30 |
| Length ratio(1) | 1.41 | | 2.14 | |
| Δm (µg/cm$^2$) | 20.4 | 27.7 | 22.3 | 35.2 |
| Δm ratio(2) | 1.36 | | 1.58 | |

**Table 1** : Nanowire lengths after 2 hours of deposition and ratios for $Bi_{2-x}Sb_xTe_3$ and $Bi_2Te_{3-x}Se_x$ derived from SEM imaging, along with measured areas under Δm curves for 10s deposition time and their ratios. (1) $l_2/l_1$ with $l_1 < l_2$. (2) $\Delta m_2/\Delta m_1$ with $\Delta m_1 < \Delta m_2$.

As can be seen in table 1, in the case of $Bi_{2-x}Sb_xTe_3$ deposits, the ratios of lengths and Δm are very close. In the case of $Bi_2Te_{3-x}Se_x$ deposits, on the contrary we observe a less good agreement between both ratios. Nevertheless, we can conclude that the deposition rate is potential dependent and is always higher at more negative deposition potentials. Qualitatively, for $Bi_{2-x}Sb_xTe_3$ the growth rate is 40 % faster at -0.3 V compared to -0.15 V, and between 60 % - 100 % faster for $Bi_2Te_{3-x}Se_x$ at -0.2 V compared to 0 V.

## Chemical composition characterization

Figure 4 presents FESEM-EDX results obtained on the samples studied in this work. They have been used to derive the stoichiometries indicated in the paper.

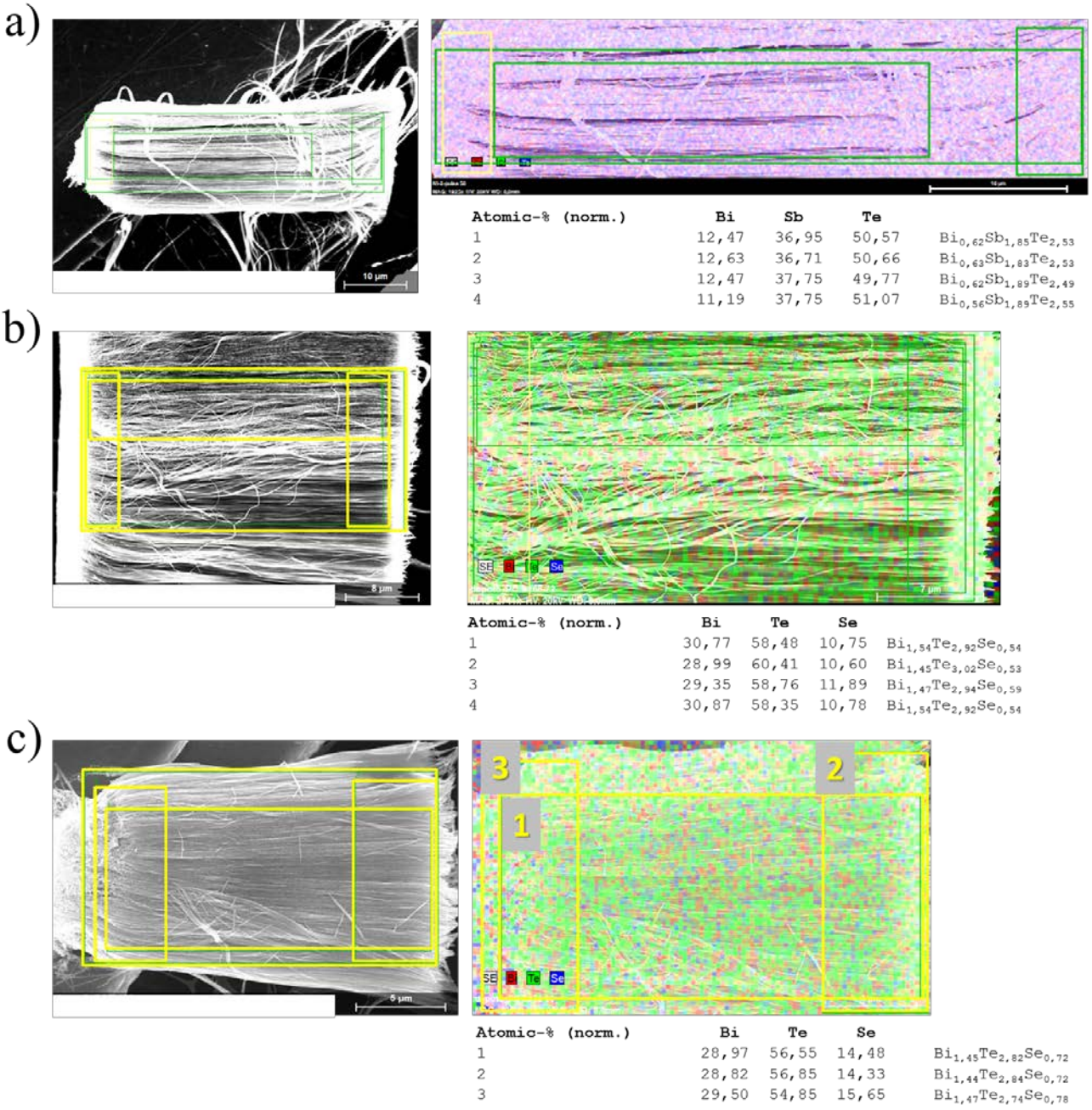


**Figure 4** : Elements distribution maps by EDX obtained on bundles of nanowires deposited in pulse potential mode. a) $Bi_{2-x}Sb_xTe_3$ deposited at -0.3 V. b) and c) $Bi_2Te_{3-x}Se_x$ deposited at 0 V and -0.2 V respectively.

**Samples used for Seebeck and electrical transport measurements**

Two types of samples have been used in this study. For Seebeck coefficient measurements, we used samples in which overgrowth was conducted until a continuous layer is formed on the template surface. This is to ensure good electrical contact between top and bottom of the nanowires in the Seebeck measurement set-up. For direct electrical transport measurements, the deposition was stopped as soon as an overgrown deposit could be observed on the perimeter of the template area exposed to the electrolyte. Figure 5 shows SEM top view images of a continuous overgrown layer (figure 5a) and of a controlled overgrowth to obtained well separated nuclei for direct nanoprobing (figure 5b). Figure 5c presents a tilted cross-section view of the template in which the thickness of the continuous layer can be seen to be less than 10 µm.

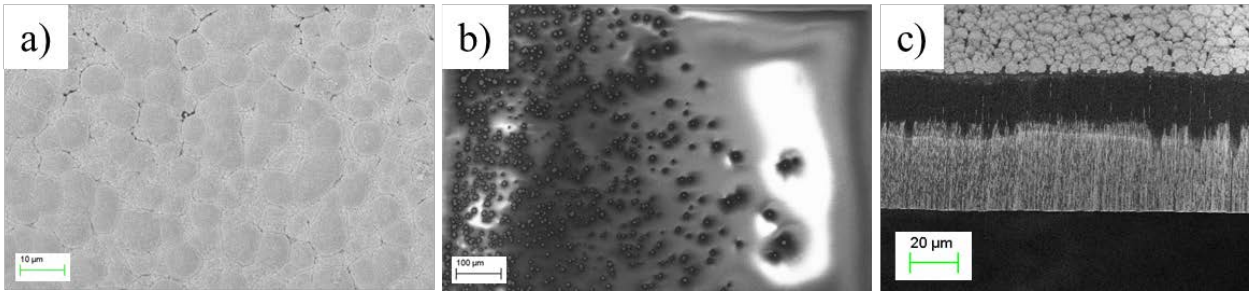


**Figure 5** : SEM top views of a continuous layer used for Seebeck coefficient measurement (a), a controlled overgrowth to obtained individual nuclei for direct nanoprobing (b), and a tilted view showing a continuous layer with thickness less than 10 µm (c).

**Structural analyses**

For the XRD measurements, the template backside was analyzed after chemical removal of gold layer.

XRD patterns (Figure 6) are in agreement with the standard patterns of p and n-type materials respectively. The $Bi_2Te_{2.7}Se_{0.3}$ and $Bi_{0.5}Sb_{1.5}Te_3$ patterns (50-0954(*) and 49-1713(Q)), reported on figure 1a and 1b respectively, confirm that the elaborated NWs are close to the expected phases. For both types and for all deposition potentials, polycrystalline NW arrays are oriented along [110] and [1 0 10] directions. $Bi_2Te_{3-x}Se_x$ NWs, deposited at low deposition rate (0 V), indicate a stronger texturing along [110] direction and peaks are highly intense. For faster

deposition rates (-0.2 V), the peaks are less intense. These results are in agreement with morphology analysis showing the same potential dependence. Slow growth rate (0 V) leads to compact and smooth NWs (Figure 1a-1) with large grain size (75 to 100 nm) and a stoichiometry of $Bi_{1.55}Te_{2.9}Se_{0.55}$. For negative deposition potential (-0.2 V), NWs have a dendritic aspect (figure 1a-2) with smaller grain size (20 to 65nm) and a higher selenium content $Bi_{1.45}Te_{2.85}Se_{0.7}$ possibly due to the faster deposition rate. BiSbTe NWs, deposited at fairly low deposition rate (-0.15 V), indicate a strong texturing along [1 0 10] with intense XRD peaks. For faster deposition rates (-0.3 V), the texturing direction is maintained but with a loss in peak intensity. These results are also in agreement with morphology analysis. Deposition potential of -0.15 V leads to compact and smooth NWs (figure 1b-1) with large grain size (100 nm) and a stoichiometry of $Bi_{0.4}Sb_{1.43}Te_{3.17}$. For faster deposition potential (-0.3 V), NWs start to lose their compact aspect (figure 1b-2) with fairly large grain size (75 nm) $Bi_{0.6}Sb_{1.85}Te_{2.55}$.

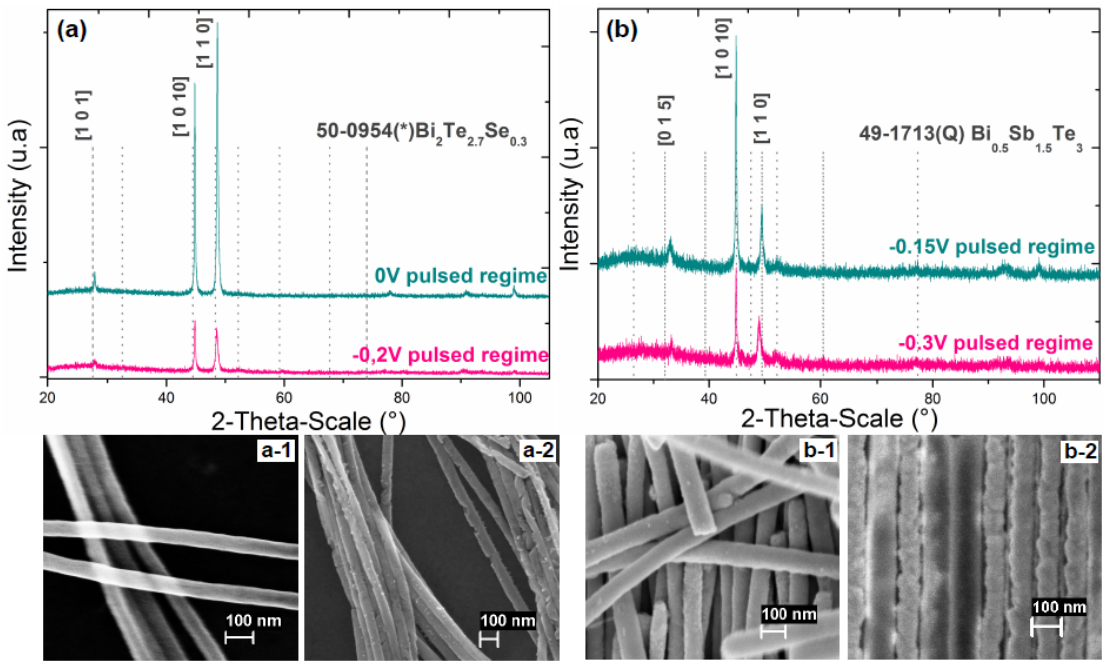


**Figure 6**. XRD patterns of as-grown nanowires and their respective SEM images of morphology observations. (a-1) $Bi_{1.55}Te_{2.9}Se_{0.55}$ NWs deposited at 0V. (a-2) $Bi_{1.45}Te_{2.85}Se_{0.7}$ NWs deposited at -0.2V. (b-1) $Bi_{0.4}Sb_{1.43}Te_{3.17}$ NWs deposited at -0.15V. (b-2) $Bi_{0.6}Sb_{1.85}Te_{2.55}$ NWs deposited at -0.3V.

Grain size was calculated using the Debye-Scherrer formula: $D = k.\lambda/\beta.cos\theta$ where $k$ is a constant of 0.89, $\lambda$ the radiation wavelength (Co Kα, λ=1.78897Å), $\beta$ is the full width at half maximum and $\theta$ the Bragg angle [4].

REFERENCES:


(1) Del-Frari, D.; Diliberto, S.; Stein, N.; Boulanger, C. ; Lecuire, J. M. *Thin Solid Films.* 483 (**2005)** 44.

(2) Masuda, H.; Nishio, K.; Baba, N. *Thin. Solid. Films*. 223 (**1993)** 1.

(3) H. Masuda, K. Fukuda. *Science.* 268 (**1995)** 1466.

(4) Cullity, B. D. *Elements of X-ray diffraction,* 2nd ed; Addison-Wesley: MA, 1978.